CNN Based Fundus Images Classification For Glaucoma Identification

Thisara Shyamalee
Department of Computer Science and Engineering
University of Moratuwa
Katubedda, Sri Lanka
thisaras@cse.mrt.ac.lk

Dulani Meedeniya
Department of Computer Science and Engineering
University of Moratuwa
Katubedda, Sri Lanka
dulanim@cse.mrt.ac.lk

2022 2nd International Conference on Advanced Research in Computing (ICARC) | 978-1-6654-0741-0/22/$31.00 ©2022 IEEE | DOI: 10.1109/ICARC54489.2022.9754171

***Abstract*—Glaucoma is a fatal, worldwide disease that can cause blindness after cataracts for people over 40-60 years. Statistics on glaucoma have shown that around 65 million people worldwide affect by glaucoma, and it is the second major reason for vision impairment after cataract. This study uses three different Convolutional Neural Networks (CNNs) architectures, namely Inception-v3, Visual Geometry Group 19 (VGG19), Residual Neural Network 50 (ResNet50), to classify glaucoma subjects using eye fundus images. In addition, several data pre-processing and augmentation techniques were used to avoid overfitting and achieve high accuracy. The aim of this paper is to comparative analysis of the performance obtained from different configurations with CNN architectures and hyper-parameter tuning. Among the considered deep learning models, the Inception-v3 model showed the highest accuracy of 98.52% for the ACRIMA fundus image dataset.**

***Index Terms*—Transfer learning, hyperparameter tuning, Inception-v3, VGG19, ResNet50**

I. Introduction

Glaucoma is a common cause of permanent blindness. It has globally affected 76 million individuals aged 40 to 80 by 2020, and the number is expected to rise to around 112 million due to the ageing population by the year 2040 [1]. However, many people do not aware of this situation as there are no early symptoms. The most prevalent chronic glaucoma condition arises when the trabecular meshwork of the eye becomes less effective in draining fluid. As this happens, eye pressure rises, leading to damage optic nerve [2]. Thus, glaucoma care is essential for sustaining vision and quality of life, as it is a long-term neurodegenerative condition that can only control [3]. Generally, glaucoma is a diagnosis utilizing fundus images of the retina. Thus the evaluation of the optic nerve is crucial in the glaucoma diagnosis process.

Deep learning (DL) is a trending computational approach used in medical imaging for image classification and segmentation in different medical applications [4]–[7]. DL-based algorithms have many promises when it comes to extracting features and discovering patterns from complex data. Several studies have been addressed glaucoma classification using DL methods with fundus images [7], [8]. A fundus image is a picture of the eye's interior through the pupil, which is the large part of an organ furthest from an opening. A picture of the back of the eye is called a retinal image, and an Optical coherence tomography (OCT) image captures the cross-section of the retina [9]. According to anatomy, the retina is a thin nerve layer that covers the rear side of the eye, and it turns light into impulses and transmits them to the brain via the optic nerve.

Although some of the studies have shown promising results [7], [8], by nature, the results are mainly dependent on the selected dataset, architecture, and hyperparameter tuning. Therefore, this study further investigates fundus image classification with several Convolutional Neural Network (CNN) architecture types to support glaucoma identification with high accuracy and optimal hyper-parameters. We design and develop three CNN architectures based on Visual Geometry Group 19 (VGG19), Residual Neural Network 50 (ResNet50) and Inception-v3. The major object of this research is to deliver an insight into a comparative study that classifies retinal images using different CNN configurations. The outcome of this study will be beneficial for the researchers and developers in the domain.

II. Literature Review

Several studies have been applied DL-based techniques to classify fundus images for the glaucoma classification process. Bajwa et al. [10], have presented a method to identify the optic disc (OD) region using three steps. Initially, they have applied the ground truth generation method to generate rectangular objects randomly. They have discovered the objects with the highest score by feeding filtered images into CNN and localized the OD region using a bounding box. Their CNN model was employed for OD classification, and the ORIGA dataset obtained an Area Under Curve (AUC) of 87.4% with a 71.2% sensitivity.

In another study, Sreng et al. [8], have suggested a glaucoma screening method using two stages. First, Optic disc segmentation has been performed using DeepLabv3+ architecture. Second, a pre-trained deep neural network has been employed for image classification. Five datasets with 2787 images have used and the ACRIMA dataset has shown an accuracy of 99.53% and AUC of 99.98%.

Moreover, Rehman et al. [7], have proposed Deep CNN architectures based two-staged glaucoma classification method.

978-1-6654-0741-0/22/$31.00 ©2022 IEEE

Four different CNN architectures namely AlexNet, Inception-v3, InceptionResNetV2 and NasNet-Large employed in the first stage. NasNet-Large performed best results for sensitivity, specificity, accuracy, AUC of 99.1%, 99.4%, 99.3%, 97.8%, respectively. Further, they have used two ensemble techniques for the public datasets ACRIMA, ORIGA-Light, RIM- ONE and two private datasets.

Another fundus image based automatic glaucoma assessment was proposed by Diaz-pinto et al. [11], and they have used five different ImageNet-trained CNN models, namely Inception-v3, XceptionNet, VGG16, VGG19, and ResNet50. During pre-processing this study has cropped the optic disc of images using a bounding box and fine-tuned the layers of the VGG16, VGG19, Inception-v3, ResNet50, and XceptionNet architectures. Then, the global average pooling layer was added instead of the fully connected layer, succeeded by the Softmax layer with two categories representing glaucoma and healthy. The VGG19 model have shown accuracy of 90.69% and VGG16, Inception-v3, XceptionNet and ResNet yielded 89.48%, 90%, 89.77% and 90.29%, respectively.

Another approach has used OCT probability map glaucoma dataset using three different CNN architectures (VGG16, ResNet18, Inception-v3) [12]. In addition, they have applied Grad-CAM visualization techniques to improve CNN performance. The VGG16 model provided the best performance with an accuracy of 95.0%, and ResNet18, Inception-v3 yielded 94.8% and 94.2%, respectively.

III. Model Design And Implementation

The high-level process view of the system is shown in Fig. 1. Our approach mainly consists of data pre-processing, augmentation, DL approach, and model evaluation. The following subsections discuss the overall process in detail.

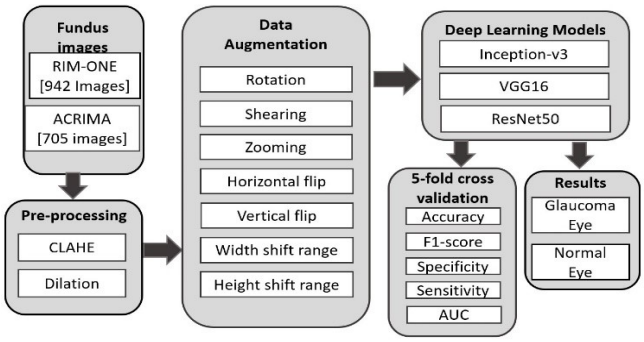

Fig. 1. Process view

A. Dataset Details

The presented method assessed on two publicly available datasets, namely RIM-ONE [13] and ACRIMA [11] dataset. RIM-ONE dataset contains eye fundus images in three versions. Versions 1 and 2 consists of 169 and 455 monosporic fundus images, respectively. Version 3 consists of 318 stereoscopic images that are categorized into four types as normal, moderate, early, and deep. Since deep, early and moderate classes belong to glaucoma status, we have considered all 3 classes as glaucoma. Thus, the RIM-ONE dataset comprises a total of 942 fundus images with 399 glaucomatous and 543 healthy subjects. The ACRIMA dataset contains 396 glaucomatous and 309 healthy subjects. During the DL process, we have split the images into a 70:15:15 ratio as training,testing and validation images, which gives the best results as per the empirical studies. Data pre-processing techniques are applied to address the imbalance of the classes and to increase the number of images in the training set for better performance.

As a sample, a healthy image is shown in Fig. 2(left), and the glaucoma image is shown in Fig. 2(right). In Fig. 2(left), the optic cup is a regular shape with a normal size neuroretinal rim, and in Fig. 2(right), the optic cup is larger with a different size neuroretinal rim than the first image.

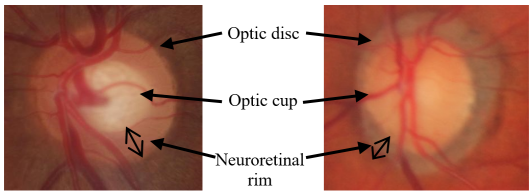

Fig. 2. Fundus image (left) healthy eye (right) glaucoma eye

B. Data Preprocessing And Augmentation

Different pre-processing techniques for medical image analysis are available in the literature [6], [14]. In this study, we have used two pre-processing techniques as dilation and Contrast Limited Adaptive Histogram Equalization (CLAHE). Dilation is a morphological operation used to improve the image's brightness and increase the size of the image [15]. CLAHE is a commonly used image processing method for enhancing image quality and contrast [16].

Generally, DL models require more data to get promising results. Thus, we applied reshaping based augmentation to address the data imbalance issue and data overfitting and used other augmentation techniques to address the data imbalance problem and to increase the number of images in the datasets. Six augmentation techniques namely rotation range of 10 degrees, shearing range of 0.2, zooming range of 0.1, horizontal flip, height shift range, and width shift range of 10% [16], are used for both datasets. Moreover, to address the class imbalance problem in the both dataset, we applied vertical flip augmentation as well, for the both dataset.

Thus, with the 70:15:15 split ratio, the training set of the RIM-ONE dataset comprises a total of 4233 fundus images with 1953 glaucomatous and 2280 healthy subjects, after applying the augmentation techniques. Moreover, the training set of the ACRIMA dataset includes a total of 3193 fundus images with 1590 glaucomatous and 1603 healthy subjects, after the augmentation process.

C. CNN Architectures

We developed different CNN architectures, with the backbones of Inception-v3, VGG19, and ResNet50 models. We compare the performance for different design models, and the two datasets separately.

Generally, CNN architectures consist of three main layers. The convolution layer is the core layer of a CNN architecture is the convolutional layer that extracts the image features on inputted images. A convolution layer usually has several convolution kernels as filters to get numerous image feature results. The pooling layer is also called the down-sampling layer, and it is the component that performs dimensionality reduction for extracted features and data compression to prevent overfitting and enhance model fault tolerance. We have used max-pooling and finally, the fully connected dense layer produces the results of the object classification function. This layer combines the feature information from each neuron in the top layer and classify images. The layers of the CNN architecture, except the last weighted layer, were maintained in a not-trainable mode to achieve optimum performance.

1) Inception-v3 Architecture: Inception-v3 is a widely used CNN architecture built by Google in 2015, which consists of 48 deep layers. Inception-v3 is a commonly used image recognition model that has been shown to attain an accuracy of more than 78.1%, and it is trained on the ImageNet dataset for 1000 classes [17]. We used the Keras API's pre-trained Inception-v3 model as the initial CNN architecture. In our approach, we have applied additional layers instead of the model's top dense layers. The global average pooling layer was placed after the Inception-v3 model to reduce the parameters, followed by the dense layer (512 units), and lastly, added the Softmax layer. It employed two neurons in the Softmax layer for normal and glaucoma categories, respectively. In order to minimize the model overfitting, add a dropout layer with 0.7 rates. Furthermore, Inception-v3 has the auxiliary classifier for tackling the problem of vanishing gradient problem. They have used a high learning rate for a model and used Adam optimizer to train the model. The fine-tuned Inception-v3 architecture is shown in Fig. 3.

2) VGG19 Architecture: VGG19 contains 19 layers, including extra convolution layers in the last three blocks. In this study, we fine-tuned the pre-trained VGG19 model. Here, the global average pooling layer is pursued by the last three newly added layers namely, dropout layer with 0.5 rates, dense layer (256 units) with ReLU activation function, and finally, Softmax layer with two outputs. Fig. 4 shows the modified diagram of VGG-19 that illustrates its architecture.

3) ResNet50 Architecture: Residual Networks (ResNet) with 50 layers has shown good performance on image recognition and localization tasks [18]. The vanishing gradient problem that occurs with utilizing a high number of layers is the main problem ResNet50 is attempting to overcome. As a result, it contains a few skip connections, allowing it to cling on data from before two layers. In this study, we have fine-tuned the pre-trained ResNet50 as follows. The last two layers, which is the dense and softmax layers are altered first. Then, the fully connected layer is substituted with another fully connected dense layer with 256 units in the same pre-trained networks. The output represents the two classes normal and glaucoma. Fig. 5 shows modified ResNet50 architecture.

We have used hyper-parameters tuning and identified the optimal parameters for training. Relu activation function is used for internal layers and batch size of 8 i used for each model training. The Inception-v3 model is trained with the learning rate of 0.0001 using the ADAM optimizer. The VGG19 and ResNet50 models are trained with a learning rate of 0.001 using the stochastic gradient descent (SGD) optimizer updates with 0.9 momentum. Since the task is binary classification (glaucoma and healthy), we adopted binary cross-entropy loss ($Loss_{BCE}$) for each model as the loss function. For N fundus images where y_i is the actual value observing a value 0 or 1 ($y_i \in \{0, 1\}$) and $p(y_i)$ is the predicted probability for the ith image. $Loss_{BCE}$ calculates the deviation between the predicted probabilities to actual class output which can be either 0 or 1. We have trained the both datasets for 150 epochs during this comparative study.

$$Loss_{BCE} = -\frac{1}{N}\sum_{i=1}^{N} y_i.\ log\ (p(y_i)) + (1 - y_i).\log\ (1 - p(y_i)) \quad (1)$$

IV. Results And Discussion

We evaluated the fine-tuned Inception-v3, VGG19, and ResNet50 models with 5-fold cross-validation with the 70:15:15 split ratio, Table I shows the data distribution of the training, testing and validation sets, where G denotes the glaucoma and N denotes the normal subjects. Overall, there are 4233 training images, 932 testing images, 926 validation images in RIM-ONE dataset and 3193 training images, 680 testing images, 674 validation images in ACRIMA dataset.

TABLE I
Data Distribution

Dataset	Train set 70%		Test set 15%		Validation set 15%	
	G	***N***	***G***	***N***	***G***	***N***
RIM-ONE	1653	2280	560	372	560	366
ACRIMA	1590	1603	372	308	366	308

The results obtained for the training accuracy, validation accuracy, training loss and validation loss for Inception-v3, VGG19 and ResNet50 models are shown in Fig. 6, Fig. 7 and Fig. 8, respectively. For each model, we have shown the obtained results for the both datasets separately. It is observable that, when the number of epochs increases from 100 to 200 the model performance becomes better and leads to a high accuracy level, avoiding overfitting. However, in general, too many and too few epochs can lead to overfitting and underfitting, respectively. Thus, early stopping is used when an arbitrary large number of epochs reach, that discontinues the performance increases on a hold out validation dataset.

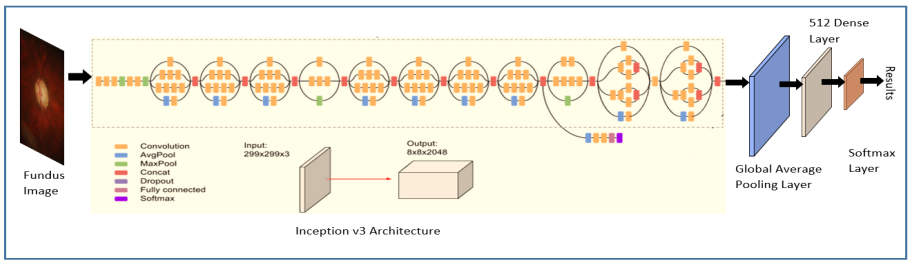

Fig. 3. Modified Inception v3 architecture

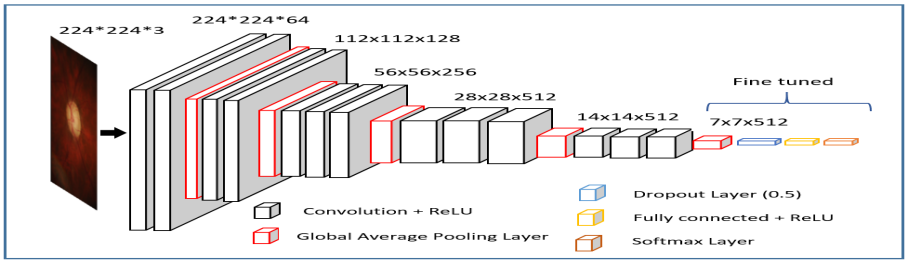

Fig. 4. Modified VGG19 architecture

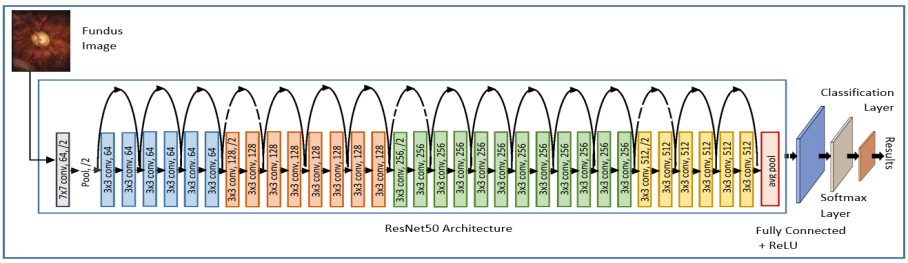

Fig. 5. Modified ResNet50 architecture

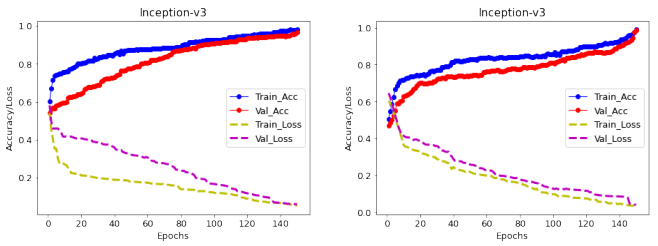

(a) (b)

Fig. 6. Results of Inception-v3 architecture on (a) RIM-ONE (b) ACRIMA

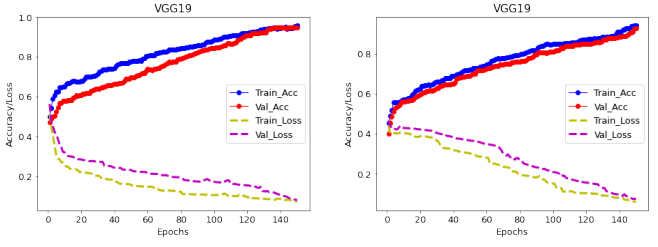

(a) (b)

Fig. 7. Results of VGG19 architecture on (a) RIM-ONE (b) ACRIMA

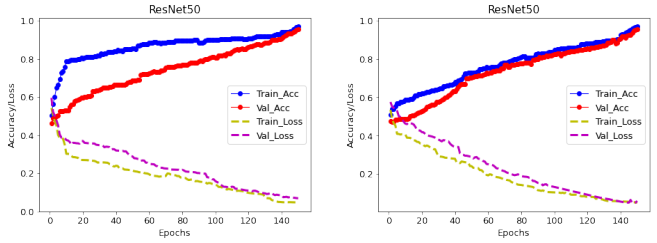

(a) (b)

Fig. 8. Results of ResNet50 architecture on (a) RIM-ONE (b) ACRIMA

Moreover, the confusion matrixes of CNN architectures based on RIM-ONE and ACRIMA datasets are shown in Fig. 9 and Fig. 10, respectively. This shows the number of correct and incorrect predictions for each class. It can be seen that all the models have yielded better predictions.

Furthermore, the Receiver operating characteristics (ROC) curves of each architecture on each dataset are plotted in Fig. 11. This shows the diagnostic ability of a binary classification for varying discrimination threshold, which is the probability of selecting a positive class over a negative class. Accordingly,

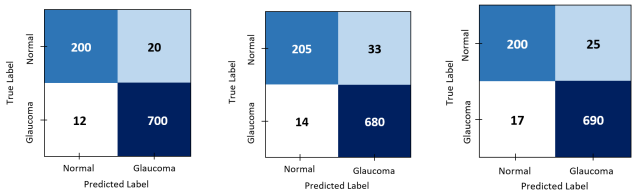

(a) (b) (c)

Fig. 9. Confusion matrix of (a) Inception-v3 (b) VGG19 (c) ResNet50 for RIM-ONE dataset

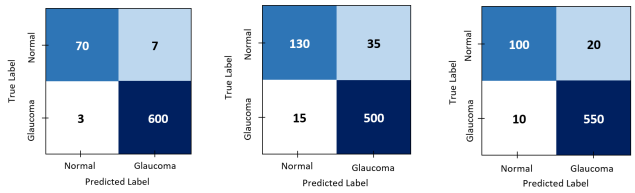

(a) (b) (c)

Fig. 10. Confusion matrix of (a) Inception-v3 (b) VGG19 (c) ResNet50 for ACRIMA dataset

it can be seen that the classifiers have given better performance with a highly accurate test since the curves are closer to the top-left corner.

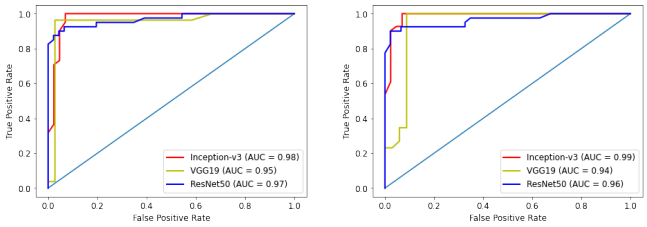

(a) (b)

Fig. 11. Results of ResNet50 architecture on (a) RIM-ONE (b) ACRIMA

In medical domain the trustworthiness of the DL model is significant. Considering the model evaluation techniques, AUC shows the diagnostic prediction quality of the model, by measuring the ability of a classifier to distinguish between classes. Moreover, sensitivity, specificity measure the probability of a positive and negative diagnostic test, respectively [19]. Thus, sensitivity is more important in medical image identification as it gives the percentage of subjects with the disease who are correctly identified by the model. We've illustrated each CNN architecture's accuracy, F1-score, precision, recall, specificity, and sensitivity obtained from the 5-fold cross-validation process. Accuracy is the total correctly identified sample, and the positive predictive value is called precision. Table II and Table III represent the performances shown by each architecture on RIM-ONE and ACRIMA datasets.

According to the performance of each CNN architecture, Inception-v3 on RIM-ONE dataset achieves 96.56% accuracy and the least test loss. Further, Inception-v3 on the ACRIMA dataset obtains 98.52% accuracy with less testing loss.

Table IV states a comparison of the proposed study with

TABLE II
PERFORMANCE OF CNN ARCHITECTURES ON RIM-ONE

Performance	**CNN Architectures**		
	Inception-v3	***VGG19***	***ResNet50***
Accuracy	96.56%	94.95%	95.49%
Precision	97.22%	95.37%	96.50%
Recall	98.31%	97.98%	97.59%
F1_score	97.76%	96.65%	97.04%
Sensitivity	98.31%	97.98%	97.59%
Specificity	90.90%	86.13%	8888%
Loss	0.0601	0.0792	0.0689
AUC	0.98	0.95	0.97

TABLE III
PERFORMANCE OF CNN ARCHITECTURES ON ACRIMA

Performance	**CNN Architectures**		
	Inception-v3	***VGG19***	***ResNet50***
Accuracy	98.52%	92.64%	95.58%
Precision	98.84%	93.45%	96.49%
Recall	99.50%	97.08%	98.21%
F1_score	99.17%	95.23%	97.34%
Sensitivity	99.50%	97.08%	98.21%
Specificity	90.90%	78.78%	83.33%
Loss	0.0414	0.0756	0.0598
AUC	0.99	0.94	0.96

the related studies. The main contribution of this research is the classification of fundus images using different CNN architectures for two datasets, with hyper-parameter tuning. We employed the dilation method which is not highlighted in most existing studies related in glaucoma classification. Furthermore, to address the class-imbalanced issues in the original datasets we performed augmentation techniques including reshaping to avoid the overfitting of the model.

Among the considered latest related studies on glaucoma classification using the RIM-ONE and ACRIMA datasets, many studies have considered VGG and ResNet architectures. The highest accuracy of 99.53% is shown by Sreng et al. [8], using the DenseNet model. They've only addressed the fact that there's a highly class imbalance in the RIM-ONE dataset but this hasn't been resolved during the research. Considering the existing literature [20], we have addressed the class-imbalances issues and applied reshaping to add more images into minor class. In our study, We experimented with several hyper parameters including optimizers and activation functions for each DL models. Thus, we obtained an accuracy of 98.52% using the inception-v3 model for the ACRIMA dataset as best results. Thus, the aim of this comparative study is achieved by producing better results using DL techniques.

V. CONCLUSION

Glaucoma is a fatal eye disease that affects millions of individuals worldwide every year. This paper presented a deep learning approaches to classify fundus images. We have proposed three fine-tuned architectures based on Inception-v3, VGG19, and ResNet50 to classify glaucoma and normal images. We have applied dilation and augmentation during data pre-processing. 5-fold cross-validation based results

TABLE IV
COMPARISON WITH EXISTING STUDIES

Study	Dataset	DL models	Optimizer	Acc. %
[11]	ACRIMA RIM-ONE	VGG16	SGD	89.48
		VGG19		90.69
		Inception-v3		90.00
		ResNet50		90.29
		Xception		89.77
[8]	ACRIMA	AlexNet	Adam	96.23
		GoogleNet		91.51
		InceptionV3		93.87
		XceptionNet		98.11
		ResNet50		95.75
		SqueezeNet		95.75
		ShuffleNet		96.23
		MobileNet		98.58
		DenseNet		99.53
		InceptionResNet		96.23
		NasNet-Large		96.23
	RIM-ONE	AlexNet	Adam	74.87
		GoogleNet		94.74
		InceptionV3		71.05
		XceptionNet		81.58
		ResNet50		92.11
		SqueezeNet		97.37
		ShuffleNet		92.11
		MobileNet		92.11
		DenseNet		94.74
		NasNet-Large		86.84
[16]	RIM-ONE	Inception-v3	Adam	92.51
[7]	ACRIMA	AlexNet	SGD	99.5
		InceptionV3		98.5
		InceptionResNetV2		99.0
		NasNet-Large		99.5
	RIM-ONE	AlexNet	SGD	87.5
		InceptionV3		92.2
		InceptionResNetV2		90.6
		NasNet-Large		94.5
This work	ACRIMA	Inception-v3	Adam	98.52
		VGG19	SGD	92.64
		ResNet50	SGD	95.58
	RIM-ONE	Inception-v3	Adam	96.56
		VGG19	SGD	94.95
		ResNet50	SGD	95.49

showed that Inception-v3 predicts glaucoma with an accuracy of 98.52% among the other convolutional neural networks architectures. This study can be extended to experiment with other possible deep learning techniques to achieve optimal results. Moreover, deep learning architectures can be designed to implement in low computational power with constrained resources, to deploy a glaucoma diagnosis support system in real-world settings.

REFERENCES

[1] W. H. Organization, "World report on vision," *World Health Organization*, vol. 214, no. 14, pp. 1–160, 2019.

[2] L. Storgaard, T. L. Tran, J. C. Freiberg, A. S. Hauser, and M. Kolko, "Glaucoma clinical research: Trends in treatment strategies and drug development," *Frontiers in Medicine*, vol. 214, pp. 1—-14, 2021.

[3] P. Harasymowycz, C. Birt, P. Gooi, L. Heckler, C. Hutnik, D. Jinapriya, L. Shuba, D. Yan, and R. Day, "Medical management of glaucoma in the 21st century from a canadian perspective," *Journal of Ophthalmology*, vol. 2016, pp. 1–22, 2016, doi: 10.1155/2016/6509809.

[4] I. Rubasinghe and D. Meedeniya, "Ultrasound nerve segmentation using deep probabilistic programming," *Journal of ICT Research and Applications*, vol. 13, no. 3, pp. 241–256, 2019, doi: 10.5614/itbj.ict.res.appl.2019.13.3.5.

[5] N. Wijethilake, D. Meedeniya, C. Chitraranjan, I. Perera, M. Islam, and H. Ren, "Glioma survival analysis empowered with data engineering—a survey," *IEEE Access*, vol. 9, pp. 43 168–43 191, 2021, doi: 10.1109/ACCESS.2021.3065965.

[6] I. Rubasinghe and D. Meedeniya, "Automated neuroscience decision support framework," in *Deep Learning Techniques for Biomedical and Health Informatics*, B. Agarwal, V. Balas, L. Jain, R. Poonia, and Manisha, Eds. Elsevier, 2020, ch. 13, pp. 305–326, doi: 0.1016/B978-0-12-819061-6.00013-6.

[7] A. U. Rehman, I. A. Taj, M. Sajid, and K. S. Karimov, "An ensemble framework based on deep cnns architecture for glaucoma classification using fundus photography," *Mathematical Biosciences and Engineering: MBE*, vol. 18, no. 5, pp. 5321–5346, 2021, doi: 0.3934/mbe.2021270 .

[8] S. Sreng, N. Maneerat, K. Hamamoto, and K. Y. Win, "Deep learning for optic disc segmentation and glaucoma diagnosis on retinal images," *Applied Sciences*, vol. 10, no. 14, pp. 1–19, 2020.

[9] H. Raja, M. U. Akram, S. G. Khawaja, M. Arslan, A. Ramzan, and N. Nazir, "Data on OCT and fundus images for the detection of glaucoma," *Data in brief*, vol. 29, pp. 1–4, 2020, doi: 10.1016/j.dib.2020.105342.

[10] M. N. Bajwa, M. I. Malik, S. A. Siddiqui, A. Dengel, F. Shafait, W. Neumeier, and S. Ahmed, "Two-stage framework for optic disc localization and glaucoma classification in retinal fundus images using deep learning," *BMC medical informatics and decision making*, vol. 19, no. 1, pp. 1–16, 2019, doi: 10.1186/s12911-019-0842-8.

[11] A. Diaz-Pinto, S. Morales, V. Naranjo, T. Köhler, J. M. Mossi, and A. Navea, "CNNs for automatic glaucoma assessment using fundus images: an extensive validation," *Biomedical Engineering Online*, vol. 18, no. 1, pp. 1–19, 2019, doi: 10.1186/s12938-019-0649-y.

[12] K. A. Thakoor, X. Li, E. Tsamis, P. Sajda, and D. C. Hood, "Enhancing the accuracy of glaucoma detection from oct probability maps using convolutional neural networks," in *Proc. International Conference of the IEEE Engineering in Medicine and Biology Society (EMBC)*, Berlin, Germany, 2019, pp. 2036–2040, doi: 10.1109/EMBC.2019.8856899.

[13] F. J. F. Batista, T. Diaz-Aleman, J. Sigut, S. Alayon, R. Arnay, and D. Angel-Pereira, "RIM-ONE DL: A unified retinal image database for assessing glaucoma using deep learning," *Image Analysis & Stereology*, vol. 39, no. 3, 2020, doi: 10.5566/ias.2346.

[14] S. De Silva, S. Dayarathna, G. Ariyarathne, D. Meedeniya, and S. Jayarathna, "A survey of attention deficit hyperactivity disorder identification using psychophysiological data," *International Journal of Online and Biomedical Engineering (IJOE)*, vol. 15, no. 13, pp. 61–76, 2019, doi: 10.3991/ijoe.v15i13.10744.

[15] H. Veena, A. Muruganandham, and T. S. Kumaran, "A novel optic disc and optic cup segmentation technique to diagnose glaucoma using deep learning convolutional neural network over retinal fundus images," *Journal of King Saud University - Computer and Information Sciences*, vol. 32, no. 2, pp. 1–12, 2021, doi: 10.1016/j.jksuci.2021.02.003.

[16] A. Singh, S. Sengupta, and V. Lakshminarayanan, "Glaucoma diagnosis using transfer learning methods," in *Proc.Applications of Machine Learning*, California, United States, 2019, pp. 1–11.

[17] C. Szegedy, V. Vanhoucke, S. Ioffe, J. Shlens, and Z. Wojna, "Rethinking the inception architecture for computer vision," in *Proc.IEEE Conference on Computer Vision and Pattern Recognition (CVPR)*, Las Vegas, USA, 2016, pp. 2818–2826, doi: 10.1109/cvpr.2016.308.

[18] K. He, X. Zhang, S. Ren, and J. Sun, "Deep residual learning for image recognition," in *Proc.IEEE Conference on Computer Vision and Pattern Recognition (CVPR)*, Las Vegas, USA, 2016, pp. 770–778.

[19] S. De Silva, S. Dayarathna, G. Ariyarathne, D. Meedeniya, S. Jayarathna, and A. M. Michalek, "Computational decision support system for adhd identification," *International Journal of Automation and Computing (IJAC)*, vol. 18, no. 2, pp. 233–255, 2021, doi: 10.1007/s11633-020-1252-1.

[20] D. M. Barros, J. C. Moura, C. R. Freire, A. C. Taleb, R. A. Valentim, and P. S. Morais, "Machine learning applied to retinal image processing for glaucoma detection: review and perspective," *Biomedical engineering online*, vol. 19, no. 1, pp. 1–21, 2020, doi: 10.1186/s12938-020-00767-2.